Available online at www.sciencedirect.com
SCIENCE DIRECT
Icarus 177 (2005) 461–471
ICARUS
www.elsevier.com/locate/icarus

Distribution of hydrate on Europa: Further evidence for sulfuric acid hydrate

R.W. Carlson [a,*], M.S. Anderson [a], R. Mehlman [b], R.E. Johnson [c]

[a] *Jet Propulsion Laboratory, California Institute of Technology, Pasadena, CA 91109, USA*
[b] *Institute of Geophysics and Planetary Physics, University of California, Los Angeles, CA, USA*
[c] *Engineering Physics, University of Virginia, Charlottesville, VA, USA*

Received 18 August 2004; revised 14 February 2005

Available online 4 June 2005

Abstract

Sulfuric acid hydrate has been proposed as an important species on Europa's surface, the acid being produced by radiolysis of surficial sulfur compounds. We investigated the spectral properties of disordered and crystalline forms of sulfuric acid and suggest that the hydration properties of Europa's hypothesized sulfuric acid lie between two end members: liquid sulfuric acid and its higher crystalline hydrates. The spectra of these end members are similar except for spectral shifts at the band edges. We measured the optical constants of sulfuric acid octahydrate and used these with simple radiative transfer calculations to fit Europa spectra obtained by *Galileo's* Near Infrared Mapping Spectrometer (NIMS). The global distribution of the hydrate that we associate here with hydrated sulfuric acid shows a strong trailing-side enhancement with a maximum fractional hydrate abundance of 90% by volume, corresponding to a sulfur atom to water molecule ratio of 10%. The hydrate concentration spatially correlates with the ultraviolet and visible absorption of the surface and with the sulfur dioxide concentration. The asymmetric global distribution is consistent with Iogenic plasma ion implantation as the source of the sulfur, possibly modified by electron irradiation and sputtering effects. The variegated distribution also correlates with geologic forms. A high spatial resolution image shows resolved lineae with less hydrate appearing within the lineae than in nearby crustal material. The low concentration of hydrated material in these lineae argues against their conveying sulfurous material to the surface from the putative ocean.

Keywords: Surfaces, satellites; Europa; Radiation chemistry; Spectroscopy; Radiative transfer

1. Introduction

Europa's surface is continuously bombarded by high-energy electrons and ions from Jupiter's energetic magnetosphere, and this flux of ionizing radiation profoundly affects the surface chemical composition. The energy flux of 7.8×10^{13} eV s^{-1} cm^{-2} absorbed in the stopping depth $D = 0.62$ mm (Cooper et al., 2001) produces a yearly dose of 640 Mrad. For comparison, the lethal dose for humans is ~400 rad (whole body exposure) and is ~15 Mrad for the radiation resistant bacteria *Deinococcus Radiodurans* (Dose et al., 1996; Duggan et al., 1963; Richmond et al., 1999; Silverman, 1991). Molecular destruction lifetimes in this radiolysis layer (of depth D) varies from a few years to 4000 years (Carlson et al., 2002). Since the optically sensed layer is comparable in depth to the radiolysis layer and radiolytic lifetimes are short compared to geological times, molecules on Europa's surface that are observed by remote optical sensing have recently suffered radiolysis. The chemical composition of the observed surface is, therefore, in radiolytic chemical equilibrium and this composition can be markedly different from the primitive unexposed mixture (Johnson et al., 2004).

Three radiolytic species identified on Europa are hydrogen peroxide (Carlson et al., 1999a), sulfur dioxide (Lane et al., 1981; Noll et al., 1995) and molecular oxygen (Hall et al., 1995, 1998; Spencer and Calvin, 2002; Spencer and

* Corresponding author.
E-mail address: rcarlson@lively.jpl.nasa.gov (R.W. Carlson).

0019-1035/$ – see front matter
doi:10.1016/j.icarus.2005.03.026

Klesman, 2001). Additionally, Europa's surface contains hydrated material indicated by distortions of H_2O absorption bands. The hydrate spectra appear to be identical over the surface, implying that only a single hydrated species is present. One candidate for this molecular species is hydrated sulfuric acid, produced and destroyed by radiolysis of sulfur-bearing material on the icy surface (Carlson et al., 1999b). It was also noted that the hydrate concentration was spatially correlated with the concentration of visually dark material, often associated with sulfur chains, S_x (Carlson et al., 1999b; Johnson et al., 1988, 2004). The hydrate distribution also correlates with SO_2 (Hendrix et al., 2002). This is consistent with the proposed radiolytic sulfur cycle, in which sulfur compounds on Europa's surface are cycled continuously to sulfuric acid, sulfur dioxide, and back to elemental sulfur (Carlson et al., 1999b). Laboratory measurements of the radiolysis and photolysis of $S_8 + H_2O$ and $SO_2 + H_2O$ ices show the formation of sulfuric acid (Carlson et al., 2002; Moore, in preparation; Moore et al., 2002; Schriver-Mazzuoli et al., 2003) with radiolytic equilibrium established in tens to hundreds of years at the expected radiation doses at Europa (Carlson et al., 2002).

The rapid cycling of sulfur-bearing compounds can hide the molecular identity of the original unexposed material. Candidates for this initial sulfurous material include sulfur ion implantation from Iogenic plasma, micrometeoroid impact, and emplacement from a possible briny or acidic subsurface Europan ocean (Kargel et al., 2000, 2001; Marion, 2002). The spatial distribution discussed here may provide clues to the origin of Europa's sulfur.

An alternative spectral identification for Europa's hydrated material has been advocated by McCord et al. (1998, 1999), who suggested that hydrated salt spectra resembled spectra of Europa's hydrated material. However many hydrated salts exhibit spectral structure in the 1.5- to 1.9-μm region (cf. Dalton et al., this issue) that is not observed in either NIMS spectra or in high-resolution telescopic observations (Spencer et al., 2005), although particular salt mixtures and thermal or radiolytic processing could diminish these spectral features (McCord et al., 2002). Since the radiolytic lifetime of sulfates is <4000 years (Carlson et al., 2002), sulfate salts would be rapidly assimilated into the sulfur cycle. In addition, a large fraction may exist as hydrated H_2SO_4 owing to the preponderance of H_2O to provide H^+, H_3O^+, and $H_2O_5^+$ cations. The salt cations may radiolytically form oxides and hydroxides, as well as salts (Johnson, 2000; Johnson et al., 2004). Based on these arguments and the spectral fits shown here, we continue to propose that Europa's hydrate spectral signature is due to hydrated sulfuric acid, with little or no discernable spectral contribution from hydrated salts.

In this work we measure the optical constants for sulfuric acid hydrate and employ them with spectral images from the *Galileo* Near Infrared Mapping Spectrometer, NIMS (Carlson et al., 1992). We use these images to map Europa's hydrate distribution, which in the following we will refer to often as the sulfuric acid distribution. We first investigated the spectral properties of disordered and crystalline forms of sulfuric acid that may exist on Europa, which differ primarily by spectral shifts at the band edges. We then measured the optical constants of frozen sulfuric acid hydrate for use in radiative transfer calculations to predict spectral radiances. Intimate mixtures of hydrated acid grains and water ice grains were assumed in the radiative transfer calculations. Using such calculations each NIMS spectrum was then fit in order to extract the acid fraction and the grain radii. The derived maps show a strong leading–trailing side asymmetry for the hydrate content, consistent with Iogenic sulfur ion implantation and radiolytic production of sulfate hydrate. The regional structure is consistent with enhanced hydrate concentrations through H_2O sublimation from diapiric and shear stress heating (Head and Pappalardo, 1999; Head et al., 1999; Nimmo and Gaidos, 2002).

2. Sulfuric acid hydrates: radiolytic production and chemical form

Radiolysis of sulfurous material in ice at Europa temperatures produces the sulfate anions and oxonium cations [H_3O^+(hydronium), $H_5O_2^+$, $H_7O_3^+$, ...] of sulfuric acid, with these ion pairs randomly distributed in the ice matrix. Their initial spatial distribution may resemble that of liquid sulfuric acid. In liquid solutions, dynamic structures called hydration shells (Ohtaki and Radnai, 1993) surround the anions and cations, with 7 to 12 H_2O molecules in the shell around a sulfate ion. More weakly bound H_2O molecules can occur in a second, outer shell. With time, the frozen mixture will transform to the lower energy state, a mixture of sulfuric acid hydrate crystallites and ice crystals. In the crystalline phase or in poorly crystalline solids, with short-range order but long-range disorder, only particular hydrates are formed. A frozen aqueous solution of H_2SO_4 produces the hydrate $H_2SO_4 \bullet nH_2O$ along with H_2O ice if the mixture is not stoichiometric. Depending upon the relative amounts of water and sulfate, hydrates with $n = 1$, 2, 3, 4, 6.5, and 8 may be formed, with the higher hydration states having higher heats of formation and, therefore, thermodynamically preferred (Zeleznik, 1991, 1994). The $n = 8$ form, sulfuric acid octahydrate, is experimentally observed to be preferentially formed in low temperature aerosols (Imre et al., 1997) and sulfuric acid is found to be much more radiation resistant at high hydration levels (Hochanadel et al., 1955). While thermal processes promote crystal formation, radiolysis will alter the crystals, primarily by removal or rearrangement of the loosely bound water molecules forming the hydrate (Nash and Fanale, 1977). Therefore, we suggest that the equilibrium arrangement of a radiolytic sulfuric acid and ice mixture is somewhere between a liquid-like state with randomly distributed anions and cations (both with hydration shells) and a mixture of water ice grains and highly hydrated sulfuric acid crystallites with $n = 6.5$ and 8 (see below).

3. Spectral properties of sulfuric acid hydrate

3.1. Spectral properties

We experimentally investigated the diffuse reflectance of the two end states mentioned above: the polycrystalline and liquid states of a sulfuric acid–water solution. Crystalline sulfuric acid hydrates contain oxonium cations so the chemical forms for the $n = 6.5$ and 8 hydrates are $(H_5O_2^+)(H_7O_3^+)SO_4^{2-}\bullet 1.5H_2O$ and $(H_5O_2^+)_2SO_4^{2-}\bullet 4H_2O$, respectively (Mootz and Merschenz-Quack, 1987). Thus, these molecules are hydrates of oxonium sulfate, with 1.5 distinct hydrated water molecules per sulfate ion in the $n = 6.5$ form and four in the $n = 8$ form. Lower hydrates, such as the $n = 4$ tetrahydrate form, $(H_5O_2^+)_2SO_4^{2-}$, are described as *anhydrous* hydronium or oxonium sulfates. Their near infrared water band spectra are expected to be different than those of the true hydrates. In earlier work (Carlson et al., 1999b) we measured the diffuse reflectance of the $n = 4$, 6.5, and 8 crystalline hydrates. Spectra for the two highest hydrates showed water-of-hydration bands, but no distinct water bands were found for the $n = 4$ hydrate (Fig. 1), consistent with the molecular forms discussed above. Clark (2004) has recently suggested that Europa's distorted water bands are due to absorption by H_3O^+ and higher oxonium ions and not by hydration water molecules. However, the lack or weakness of such features in the spectrum of $H_5O_2^+$-bearing tetrahydrate (Fig. 1) may be inconsistent with this interesting hypothesis. In the temperature range from 77 K to melting (~210 K) the reflectance spectra for the $n = 8$ and 6.5 hydrates were identical; spectra for the $n = 8$ case are shown in Fig. 1.

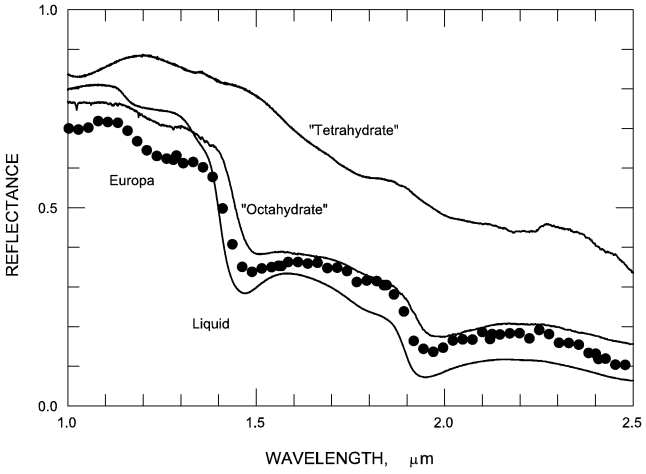

Fig. 1. Diffuse-reflectance spectra of solid and liquid sulfuric acid and Europa. Radiolytically produced sulfuric acid may have a random, liquid-like distribution of cations and anions and its spectrum may resemble that of liquid H_2SO_4, shown here for an 8:1 H_2O:H_2SO_4 solution at ~210 K. With time, the random sulfuric acid arrangement may crystallize into hydrates. The liquid spectrum and the crystallized "octahydrate" $[(H_5O_2^+)_2SO_4^{2-}\bullet 4H_2O]$ spectrum are similar to spectra of Europa's hydrated material. The "tetrahydrate" $[(H_5O_2^+)_2SO_4^{2-}$, not a true hydrate but considered to be anhydrous oxonium sulfate] shows weak or no distorted water bands. The Europa NIMS spectrum (from G1ENNHILAT01, sample 27, line 32) provides a qualitative comparison but is not comparable in detail since there are differences in grain size, H_2O content, and observing geometry. Quantitative comparisons are performed in this work using measured indices and radiative transfer fits.

Spectra for the random, liquid-like case may be represented by spectra of liquid sulfuric acid. The spectrum of an $n = 8$ solution at a temperature just above melting (Fig. 1) is similar to the frozen octahydrate, except in the vicinity of the band edges, where the minima are shifted to shorter wavelengths by ~0.05 μm in going from the crystalline to the disordered state. Similar shifts, in both direction and magnitude, were observed in proton-irradiated sulfate hydrates (Nash and Fanale, 1977). We therefore assume that Europa's sulfuric acid hydrate will exhibit a radiolytic equilibrium lying between the ordered and disordered states, and will possess optical properties intermediate between the frozen and liquid cases (Fig. 1).

In this work we use optical constants derived for the octahydrate/hemihexahydrate case (see below), anticipating that the radiative transfer solutions based on these optical constants will be inaccurate at the band edges. The positions of band minima and band edges are experimentally observed in the laboratory to be different for disordered and crystalline sulfuric acid (Fig. 1) and for unirradiated and irradiated sulfate hydrates (Nash and Fanale, 1977). We hypothesize that the band minima and band edge wavelengths for a hydrate on an irradiated surface are in general *not* the same as those for the unirradiated hydrate. Furthermore, hydrate bands are sufficiently broad that unique identifications are not possible. However, the overall shapes of hydrate bands are different for different hydrates, so accurately matching overall shapes can instill confidence in a proposed identification.

3.2. Infrared optical constants

Our radiative transfer method (see next section) uses the wavelength dependent optical constants $\tilde{m} = m + ik$ to calculate predicted radiances. To obtain the imaginary component k we measured the absorption coefficient for $H_2SO_4\bullet 8H_2O$. Stoichiometric mixtures of H_2SO_4 and H_2O were prepared using JT Baker reagent grade H_2SO_4 and deionized water (resistivity > 17 MΩ cm) that was filtered using a 0.2 μm filter. Dissolved gas that could form bubbles that scatter light in a wavelength dependent fashion was removed by bubbling helium gas through the sample. The solutions were introduced into quartz absorption cells, slowly frozen, and then maintained at ~77 K using liquid nitrogen. Cells with ~0.1 and 1 mm path lengths were used to measure the large range of absorptivity without exceeding the dynamic range of the detection system. A Cary Model 5E spectrometer was used to measure the transmission between 0.9 and 2.5 μm with a resolution of 1 nm. Absence of wavelength dependent scattered light was verified by uniform spectral transmission in the short wavelength region where the absorption coefficient value is effectively zero. No measurable interference fringes were pro-

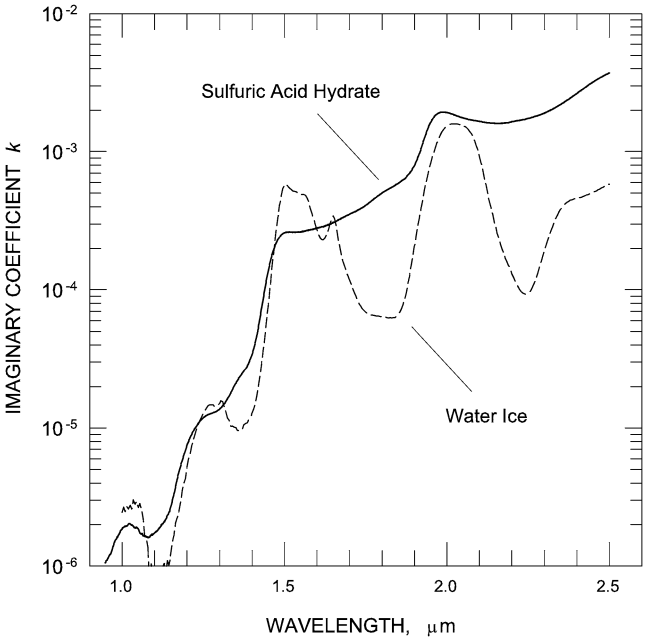

Fig. 2. Imaginary coefficient of the infrared optical constants for sulfuric acid octahydrate and water ice at 120 K. The sulfuric acid results were obtained in this work; the H_2O values are from Grundy and Schmitt (1998).

duced by either cell. The path length of the 1-mm cell is known to better than 5% and the absorption coefficient measured at 1.5 μm using this cell was then used to calibrate the thickness of the 0.1-mm cell. The measured absorption coefficients α were used to derive the imaginary part of the complex index $k = \alpha\lambda/4\pi$ (Fig. 2). The uncertainty in the pathlength of the 1-mm cell leads to an overall (scaling) uncertainty of ∼5%. At short wavelengths the possible errors in k are $\sim 2 \times 10^{-7}$ due to uncertainty in the unit transmission level. The real component m was found by Kramers–Kronig inversion (kindly performed by Carly Howett, Oxford University). The long-wavelength starting value was obtained using m for cold liquid sulfuric acid at 2.5 μm (Tisdale et al., 1998) and corrected for the density difference between the liquid and solid forms. Values for the imaginary coefficient k are shown in Fig. 2 and compared with those of H_2O ice at 120 K (Grundy and Schmitt, 1998; Schmitt et al., 1998).

4. Radiative transfer formulation and spectral fits

4.1. Radiative transfer

Having determined the optical constants for frozen sulfuric acid hydrate, and using Grundy and Schmitt's optical constants for H_2O ice at 120 K [representative of Europa's daytime temperature (Spencer et al., 1999)] we can compute comparison spectra and determine the fractional concentration and grain radii for each pixel in the NIMS spectral images. Theoretical reflectance spectra are computed by assuming intimate granular mixtures of hydrate grains and ice grains with the acid and ice grain radii denoted by r_A and r_I, respectively. For the two types of grains, we compute single scattering albedos (ϖ_A and ϖ_I) and asymmetry parameters (g_A and g_I), the latter being the intensity-weighted integral of the cosine of the scattering angle (Van De Hulst, 1980a). These quantities are computed using the geometric optics approximation by performing ray traces through spheres with relevant values of $m(\lambda)$, $k(\lambda)$, and r. We treat the narrow-angle diffracted rays as a non-deviated component of the incident radiation. This geometric approximation is appropriate for $2\pi r/\lambda \gg 1$, which we will find below is approximately true for Europa's surface grains.

The single scattering albedos are combined to form the effective value $\langle\varpi\rangle$ by weighting the individual values by the absorption cross section πr^2 and number densities $\mathcal{N}$:

$$\langle\varpi\rangle = \frac{\pi r_A^2 \mathcal{N}_A \varpi_A + \pi r_I^2 \mathcal{N}_I \varpi_I}{\pi r_A^2 \mathcal{N}_A + \pi r_I^2 \mathcal{N}_I}.$$

The effective asymmetry parameter $\langle g\rangle$ is found by weighting by the relative amount of light singly scattered:

$$\langle g\rangle = \frac{\pi r_A^2 \mathcal{N}_A \varpi_A g_A + \pi r_I^2 \mathcal{N}_I \varpi_I g_I}{\pi r_A^2 \mathcal{N}_A \varpi_A + \pi r_I^2 \mathcal{N}_I \varpi_I}.$$

Solutions for arbitrary phase functions and single scattering albedos are not available, but we can use Van De Hulst's (1980b) similarity relations to determine the equivalent single scattering albedo ϖ_E and asymmetry parameter g_E for which solutions are available. In order to approximate the strong forward scattering of refracting grains, we used the forward scattering Euler phase function $p_E(\Theta) = 1 + \cos(\Theta)$, where Θ is the scattering angle. (Results using the Euler phase function are nearly identical to those obtained using isotropic scattering.) Since the asymmetry parameter for the Euler phase function is $g_E = 1/3$, the similarity relations

$$\frac{1-\varpi_E}{1-(1/3)\varpi_E} = \frac{1-\langle\varpi\rangle}{1-\langle g\rangle\langle\varpi\rangle}$$

determine ϖ_E. Approximate solutions are computed using the isotropic case but replacing the singly scattered component with $p_E(\Theta)$ (Carlson and Judge, 1976; Hapke, 1981). Radiances I are calculated as

$$I = \pi F\left(\frac{1}{4\pi}\right)\frac{\mu_0}{\mu+\mu_0}\varpi_E\big[H(\mu)H(\mu_0) - 1 + p_E(\Theta)\big],$$

where μ_0 and μ are the cosines of the incidence and emission angles, respectively, and πF is the solar irradiance. This formulation provides a good approximation to Chandrasekhar's exact solution (Hapke, 1981). The H functions are calculated using Hapke's approximation $H(\mu) = (1 + 2\mu)/(1 + 2\gamma\mu)$, where $\gamma = \sqrt{(1-\varpi)}$ (Hapke, 1981). We use the radiance factor $R = I/(\mu_0 F)$ (Hapke, 1993) in the inversions.

4.2. Spectral inversion procedures

Theoretical radiance factor spectra were computed using the above method and values of r_A, r_I, and f, the volume hydrated sulfuric acid fraction, where $f = [H_2SO_4 \bullet nH_2O]/([H_2SO_4 \bullet nH_2O] + [H_2O])$ and the brackets denote molecular number densities. Spectra were computed at a resolution 3× higher than the NIMS instrumental resolution (0.025 μm, FWHM) and then convolved to the measured NIMS triangular slit function (Carlson et al., 1992).

Our laboratory-derived optical constants extend from 1 to 2.5 μm and the NIMS instrument had its full capability over this wavelength range early in Galileo's orbital mission. However the detector (No. 3) that covered the 1 to 1.3 μm interval became inoperative in the third orbit. In order to perform a consistent inversion analysis we used only data from detectors common to all of the data sets and within the range of experimental indices, thereby limiting the inversion computations to 1.3 to 2.5 μm. The absolute calibration of the NIMS instrument is uncertain to ±10% (Carlson et al., 1992) and, since we are interested in the spectral shape rather than the precise level, we normalized each computed spectrum to the corresponding observed spectrum using a multiplicative factor c that minimized the variance $\sigma^2 = \sum(R_{obs} - cR_{calc})^2/(N-1)$. Here R_{obs} and R_{calc} are observed and calculated radiance factors and N is the number of NIMS wavelength channels used in the inversion computation. Following our hypothesis that band minima and edge positions are altered by radiation, narrow regions at the band edges were not used to compute the variance and influence the fit. The same radiation-induced shifts observed in the laboratory (discussed previously) are very likely to occur on this heavily bombarded satellite and produce shifts that we cannot yet characterize due to the lack of appropriate irradiation-experiment data.

For each NIMS spectrum, with its associated incidence and emission angles, we first computed normalized spectra for a three-dimensional array of the parameters r_I, r_A, and f. The variance was computed for each spectrum, and the values of the array-search parameters where σ^2 was a minimum were used as the starting parameters for a higher-precision grid search (Bevington, 1969). For regions exhibiting high values of f (i.e., the trailing side observations from G1) the grid-search sensitivity to the ice radius was low, so we accepted the array-search value for r_I and performed a grid search for only r_A and f. Three-dimensional grid searches were performed for the other data sets. The grid search proceeded by minimizing σ^2.

Results for three regions on Europa's trailing side with different fractional content f are shown in Fig. 3. The standard deviations σ between the observed and calculated spectra generally were found to be <1% in radiance factor. The observed band edges are shifted toward shorter wavelengths compared to the fitted spectra, consistent with radiolytic production and modification of sulfuric acid hydrate as discussed above. The amount of shift is greatest for material

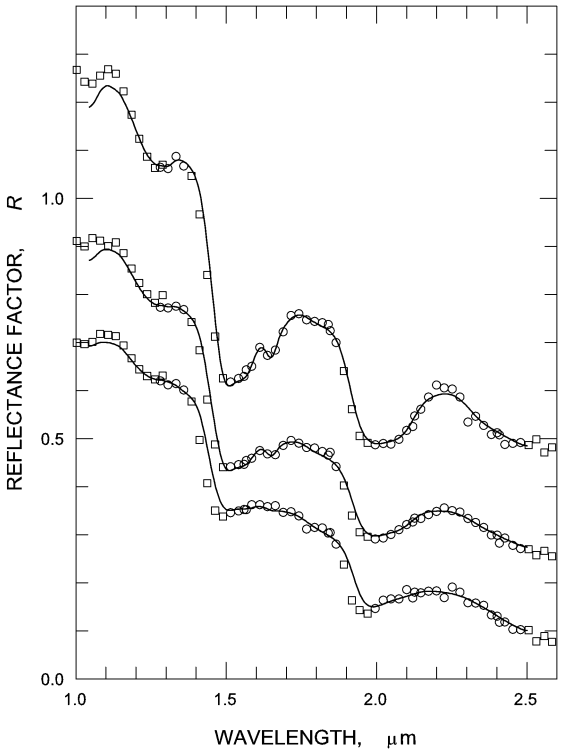

Fig. 3. Example fits to NIMS spectra of Europa. Spectra from the G1-ENNHILAT01 observation for three different concentration ratios illustrate the quality of the radiative transfer fits. From top to bottom, the concentration fractions f are 0.30, 0.54, and 0.89, respectively. Corresponding values for the ice and acid grain radii, all in μm, are $r_I = 104$, 90, 27 and $r_A = 9.5$, 7.0, 6.2. To ensure uniform analyses with the entire dataset and to account for likely but unknown radiation-induced shifts, only the circled data points were used to fit the data (see text). Specifically, for the datasets used (Table 1), the data from detector-3 ($\lambda < 1.3$ μm) were obtained only in G1 and, to be consistent with the other fits, were not used for deriving the fitted spectra. However, they can be used to judge the extrapolated fit. The data points at the band edges were not used in the fitting procedure due to likely, but unknown, radiation-induced shifts (see text). The standard deviations are $\sigma < 1\%$ for these spectral fits.

with the highest fraction f, as expected, but the magnitude of the shift is small compared to the disordered case (liquid H_2SO_4, Fig. 1), as might occur if sulfuric acid hydrate is present as radiation-altered crystalline or poorly-crystalline aggregates.

5. Surface distribution: results and discussion

5.1. Global distribution

We used Galileo NIMS data from observations obtained during the G1, E6, E15, and E17 orbits (Table 1) to derive the global concentration of the assumed hydrated H_2SO_4 (Fig. 4, top panel). The results show an asymmetric global pattern with regional variations associated with lineae and disrupted terrain. The highest concentration was found in the trailing hemisphere, with $f \sim 0.9$. The leading hemisphere, at least for the portions observed, shows little hydrate ($f \sim 0.1$), giving a strong leading–trailing side asymmetry.

Table 1
NIMS observations used for global mapping (Fig. 4) and a regional map (Fig. 6). The latitude and longitude ranges are approximate and the phase, incidence, and emission angles refer to the center of the observation. Detector 3, covering the 1 to 1.3-μm region, was operative only for the first of the listed observations and not used for inversion analysis

Observation	Latitudes	Longitudes	Scale (km/pixel)	Phase angle	Incidence	Emission	Notes
G1ENNHILAT01	30° S–90° N	150° W–300° W	39	31	19	16	Global
E6ENTERINC01	39° S–34° N	132° W–255° W	23	36	28	9	“
15ENSUCOMP03	5° S–7° N	90° W–120° W	7	103	55	48	“
17ENGLOBAL02	80° S–80° N	85° W–150° W	29	101	75	27	“
15ENREGION01	4.5° N–9.7° N	182° W–187° W	1.7	53	34	19	Regional

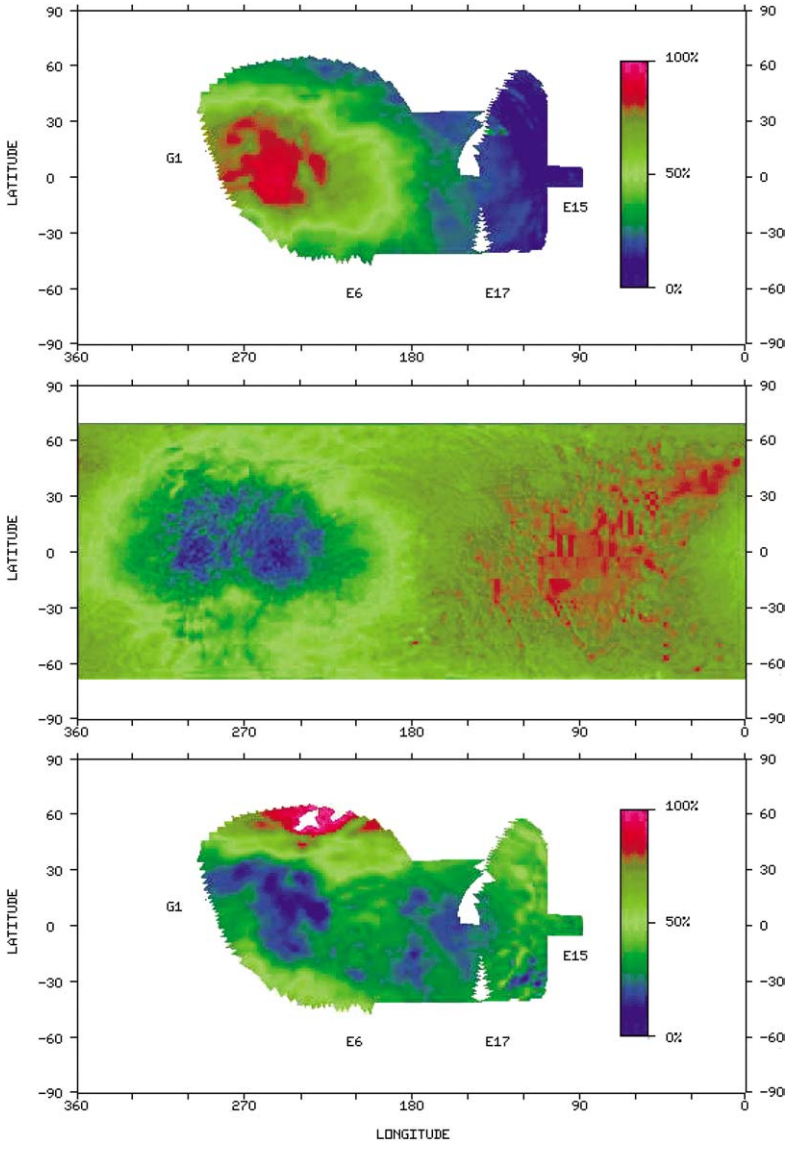

Fig. 4. Global distribution of hydrate and ultraviolet and infrared albedos. Top panel: distribution fraction f of assumed hydrated sulfuric acid. Middle panel: Voyager UV/V ratio map, from McEwen. Bottom panel: NIMS 0.7 μm/1.2 μm ratio map, scaled. Note the trailing side enhancement of sulfuric acid hydrate and its correlation with UV and 0.7 μm absorption.

The trailing side “bulls-eye” distribution is longitudinally centered on the orbital anti-apex (270° W) but latitudinally offset from the equator to the north by ∼5°. The latitudes at 270° W for which the concentration is half the maximum value are ∼ −30° and 40°. In the eastern direction, the half-concentration point on the equator is at ∼190° W. We have insufficient coverage of Europa to describe the complete distribution, but if the trailing side distribution is symmetric about the anti-apex, then the corresponding western half-concentration point would be at ∼350° W. The full width

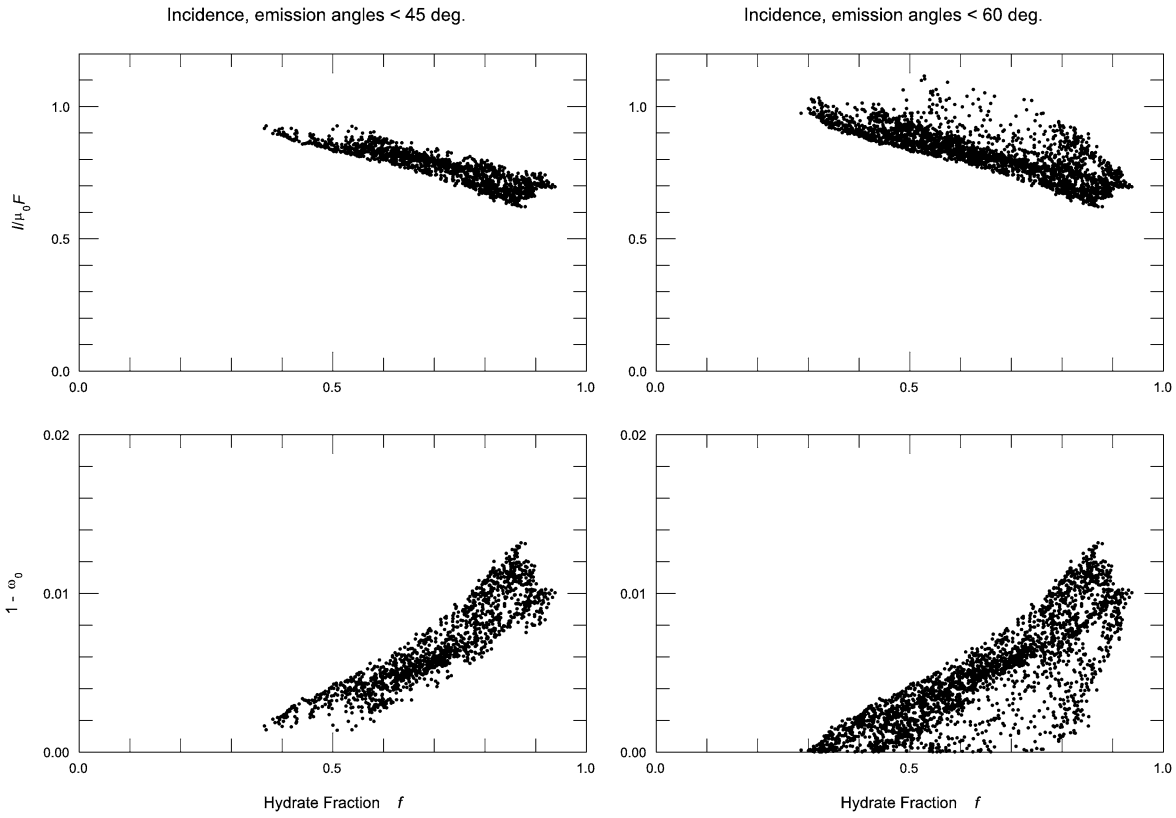

Fig. 5. Correlation of 0.7 μm radiance factor and the single-scattering absorption, $1 - \varpi_0$ as a function of the hydrate concentration f. Two different incidence and emission angle ranges are considered. The left panels are for both angles 0–45° while the right-hand panels are for 0–60°. The differences in the correlation plots for these different cases may indicate vertical variations in the hydrate or 0.7-μm absorber, presumed to be sulfur chains and polymers.

and height at half-concentration are then 160° and 70°, respectively.

The derived hydrate concentration map is similar to the UV/V ratio images derived by McEwen (1986) (Fig. 4, middle panel), where the blue regions in the Voyager map correspond to a UV absorbing material suggested by McEwen to be exogenic and possibly sulfur from Iogenic ion implantation. The hydrate concentration is also similar to the NIMS 0.7-μm albedo map (Fig. 4, bottom panel), and consistent with an absorbing species such as long-chain sulfur polymers that absorb to >1 μm (Hosokawa et al., 1994). This correlation is illustrated in Fig. 5, where the 0.7 μm radiance factor and corresponding single-scattering absorption (the complement of the single scattering albedo, $1 - \varpi$) are plotted as a function of the fraction f derived here. The surface is more absorbing at 0.7 μm for higher values of f obtained from our analysis of the hydrate bands, with $1 - \varpi \sim 0.01$ for $f \sim 0.8$. The correlation depends somewhat on the incidence and emission angles. Since higher incidence and emission angles probe less deeply into the medium, this dependence may indicate vertical structure in the optically-sensed layers.

The hydrate fraction f also correlates with SO_2 concentrations derived by Hendrix et al. (2002) and the observed SO_2 column density is within a factor of two of that predicted using laboratory radiolysis production and destruction rates (Carlson et al., 2002). This suggested association of sulfuric acid hydrate with sulfur and sulfur dioxide is a natural consequence of the radiolytic sulfur cycle (Carlson et al., 1999b, 2002).

The inferred hydrated sulfate reaches a concentration of $f = 0.9$ on the trailing side apex, giving an approximate ratio of one equivalent sulfur atom per ten water molecules at the surface. Ion implantation from the Iogenic sulfur–oxygen plasma can provide more than enough sulfur to account for this inferred amount of sulfur. The flux of sulfur ions at the trailing side apex is $\sim 1.4 \times 10^8$ cm^{-2} s^{-1} (Johnson et al., 2004), depositing a 1-mm thick layer in 1 My in the absence of plasma deflection, gardening, or asynchronous rotation. For a 10-My old surface (Zahnle et al., 1998, 2003) that is impact gardened at the rate used in Cooper et al. (2001), corrected for the leading–trailing impact asymmetry (Zahnle et al., 1998), an equivalent sulfur atom to water ratio [S]/[H_2O] ~ 0.3 was estimated for the surface of the trailing side regolith (Carlson et al., 2000). Plasma deflection or asynchronous rotation could reduce this concentration to the observed value. The global concentration profile resembles the predicted deposition pattern (Johnson et al., 1988).

The trailing-side hydrate concentration also resembles the pattern of energy deposition from precipitating electrons

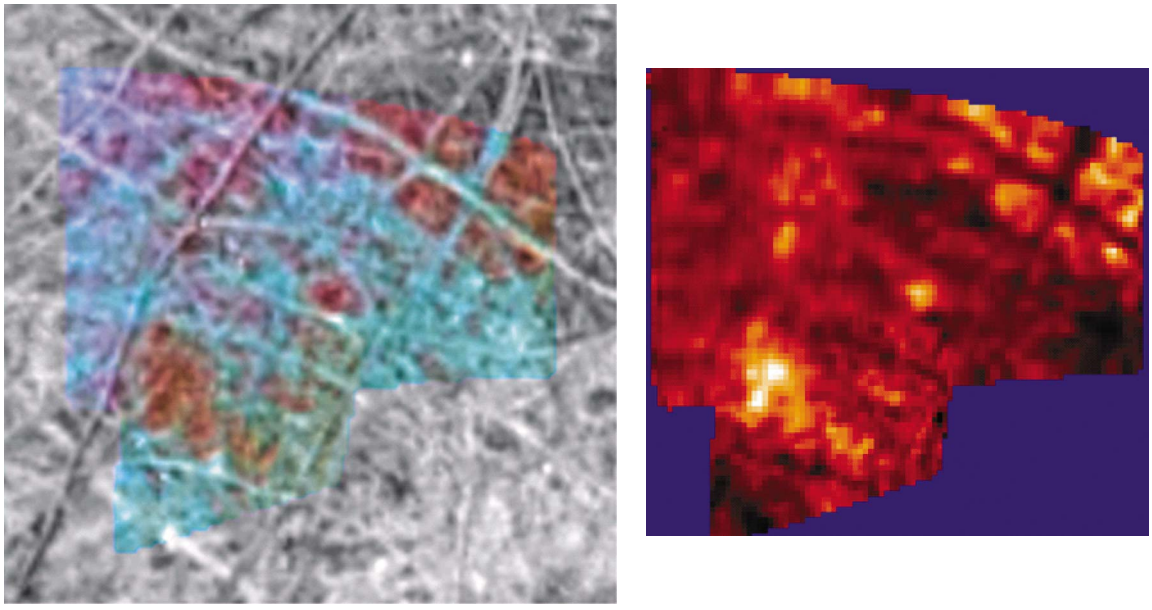

(a) (b)

Fig. 6. High resolution regional concentration map. (a) A false color NIMS image overlain on a higher-resolution Galileo SSI image (mosaicked by R. Pappalardo). The NIMS observation region extends from 182° to 188° W longitude and between 4° and 10° N latitude. The false color image depicts icy regions as blue and hydrated material as red. (b) Sulfuric acid fractional concentration map. The concentration range is from $f = 0.2$ to 0.5. Note the lower concentration in the lineae.

(Paranicas et al., 2001), which is expected to be non-uniform (in contrast, proton irradiation is nearly uniform across the surface). However, if radiolysis both produces and destroys sulfuric acid on relatively short time scales, then in steady state its concentration should be approximately independent of the flux of incident ionizing energy and indicative of the total sulfur content. Differences in relative production and destruction rates between electron and proton irradiation may play a role in producing this "bullseye" feature.

An explanation for Europa's hemispheric color difference, which is shown here to be correlated to the hydrate concentration profile, has been proposed by Tiscareno and Geissler (2003). They suggest that water molecules preferentially sputtered from the trailing side can coat the leading side and cause the observed color difference. They compute a coating rate on the leading side of 0.003 $\mu m\,yr^{-1}$. However, this is much slower than the burial rate from micrometeorite gardening of $\sim 1\ \mu m\,yr^{-1}$ (Cooper et al., 2001), so instead of providing an ice surface covering, this process will slightly increase the water content of the gardened regolith. Therefore, sputtering redistribution is not robust enough to explain the trailing–leading side asymmetry.

Another explanation for the color asymmetry is from asymmetric emplacement of sulfurous material from the putative ocean, a suggestion prompted by the young chaotic terrain present on the trailing side. However, the leading side also exhibits extensive chaotic terrain, so other processes must be operating if this hypothesis is to be viable. Recent analyses of Galileo images for cryovolcanism indicate no widespread effusion of material from below (Fagents, 2003).

5.2. Regional variations, an example

The global image (Fig. 4) suggests a variegated concentration profile that is related to local geological features. Higher resolution NIMS maps verify this notion. An example is shown in Fig. 6, which was obtained during the E15 orbit and is one of the highest resolution maps of Europa obtained by NIMS. The mapped area occurs in the anti-jovian hemisphere, a region containing numerous linear and arcuate bands, some of which were resolved by NIMS.

Most lineae observed by NIMS during the mission were unresolved, giving the impression that the entire linea contains hydrated material and could have been a source of outflowing material from the putative ocean. However, several lineae cutting through the observation are sufficiently resolved to provide an alternate description. Comparing the acid fraction map (Fig. 6b) with the context map (Fig. 6a) one finds that resolved lineae, for example the two intersecting lineae at upper right and the broad linea at lower left, contain less hydrate than the surrounding margins and plains. If the lineae were the sources of sulfate brines from an ocean, then the opposite compositional difference might be expected. The source material, that material filling the cracks in the center of the lineae, would possess more hydrated material compared to the icy margins. While this observation argues against an endogenic source of sulfurous or hydrated material, the small number of lineae examined here may not be representative of all lineae. In addition, ridge formation mechanisms are not well understood nor are the processes affecting lineae after their formation, leading to their brightening with time.

The high concentration of hydrate in the crustal margins may arise as a sublimational lag deposit (Fagents et al., 2000; Head et al., 1999). Heating of the surface will preferentially sublimate H_2O since its vapor pressure is much higher than the vapor pressures of S_x and H_2SO_4, and even modest heating can saturate and then darken a surface. It has been suggested that warm ice diapirs, upwelling in linear cracks, can heat and sublimate the adjacent crust to form diffuse margins of dark refractory material (Head et al., 1999). Another heating mechanism is frictional shear heating by strike-slip motion (Nimmo and Gaidos, 2002).

6. Summary and outstanding issues

Here we give further laboratory support for our interpretation that Europa's hydrate is a radiolytically produced sulfuric acid hydrate. We measured the imaginary index of frozen sulfuric acid octahydrate to invert Galileo NIMS Europa spectra and estimated the abundance distribution of the hydrate. Although ionizing radiation at Europan conditions is known to produce shifts in band minima and band edges, the laboratory measurements are for unirradiated polycrystalline sulfuric acid. Additionally, radiolytically produced sulfuric acid hydrate is unlikely to be a crystalline hydrate until it is thermally annealed. It would more likely have randomly distributed anion and cation pairs similar to the ion distribution of liquid sulfuric acid. Fortunately, liquid and crystalline sulfuric acid hydrate exhibit similar spectra, except at the band edges and band minima where spectral shifts occur between the two states. Therefore we hypothesize that radiolytic production and modification alters the spectra in these regions relative to unirradiated samples. The magnitude of these shifts are currently unknown. If this is true, then the measured indices near the band edges and minima are not representative of irradiated sulfuric acid. In using optical constants to fit several sets of the Galileo NIMS observations, we did not use data in the suspect regions. From this consistent analysis we obtained the following parameters: ice and hydrate grain radii and hydrate fraction.

The two-component mixture of ice and hydrated sulfuric acid grains provides good fits to the overall shape of Europa's spectrum in the 1–2.5 μm region. This reinforces our proposal that the observed hydrate is a sulfuric acid hydrate that is produced by radiolytic processing of sulfur in ice. Work is still needed for the spectral regions we ignored. In these regions shifts occur which we hypothesize are due to radiolytic production effects and radiation-induced defects. Confirming this will require new experiments in which appropriate mixtures are exposed to varying amounts of ionizing radiation and their near-infrared optical properties determined. This set of experiments is being prepared in our laboratory.

The derived hydrate abundance and distribution is also seen to be consistent with Iogenic sulfur ion implantation. However, the relative importance of exogenic and endogenic sources of sulfurous material to Europa's surface is still unresolved. Clues were found by examining a few lineae. These may be eventually strengthened by examining more regions and by looking for correlation of the hydrate (and associated dark material) with geological structures. While some of these associations may be explained by heating effects that do not require extrusion of subsurface material, other constructs (e.g., the wedges) may provide valuable constraints. The relationship between composition and ridge mass wasting merits examination.

Acknowledgments

We thank the reviewers for careful reviews and many suggestions, Marla Moore and Reggie Hudson for valuable discussions about radiolytic processes and radiation chemistry, Joel Mosher for mosaicking the concentration maps, Bob Pappalardo for the NIMS/SSI overlay map, Bernard Schmitt for providing ice optical constants, Carly Howett for the Kramers–Kronig analysis, and Alfred McEwen for his Voyager map data. Frank Leader's diligent work on the NIMS calibration is gratefully appreciated. This work was supported by NASA's Planetary Geology and Geophysics Program. Portions of the research described in this paper were carried out at the Jet Propulsion Laboratory, California Institute of Technology, under a contract with the National Aeronautics and Space Administration.

References

Bevington, P.R., 1969. Data Reduction and Error Analysis for the Physical Sciences. McGraw–Hill, New York.

Carlson, R.W., Anderson, M.S., Johnson, R.E., 2000. Radiolytic production and destruction of sulfurous compounds on Europa (abstract). Eos Trans. AGU 81 (48), F793.

Carlson, R.W., Anderson, M.S., Johnson, R.E., Schulman, M.B., Yavrouian, A.H., 2002. Sulfuric acid production on Europa: The radiolysis of sulfur in water ice. Icarus 157, 456–463.

Carlson, R.W., Anderson, M.S., Johnson, R.E., Smythe, W.D., Hendrix, A.R., Barth, C.A., Soderblom, L.A., Hansen, G.B., McCord, T.B., Dalton, J.B., Clark, R.N., Shirley, J.H., Ocampo, A.C., Matson, D.L., 1999a. Hydrogen peroxide on the surface of Europa. Science 283, 2062–2064.

Carlson, R.W., Johnson, R.E., Anderson, M.S., 1999b. Sulfuric acid on Europa and the radiolytic sulfur cycle. Science 286 (5437), 97–99.

Carlson, R.W., Judge, D.L., 1976. Pioneer 10 ultraviolet observations of Jupiter: The helium to hydrogen ratio. In: Gehrels, T. (Ed.), Jupiter. University of Arizona Press, Tucson, pp. 418–420.

Carlson, R.W., Weissman, P.R., Smythe, W.D., Mahoney, J.C., Aptaker, I., Bailey, G., Baines, K., Burns, R., Carpenter, E., Curry, K., Danielson, G., Encrenaz, T., Enmark, H., Fanale, F., Gram, M., Hernandez, M., Hickok, R., Jenkins, G., Johnson, T., Jones, S., Kieffer, H., Labaw, C., Lockhart, R., Macenka, S., Marino, J., Masursky, H., Matson, D., McCord, T., Mehaffey, K., Ocampo, A., Root, G., Salazar, R., Sevilla, D., Sleigh, W., Smythe, W., Soderblom, L., Steimle, L., Steinkraus, R., Taylor, F., Wilson, D., 1992. Near-infrared mapping spectrometer experiment on Galileo. Space Sci. Rev. 60 (1–4), 457–502.

Clark, R.N., 2004. The surface composition of Europa: Mixed water, hydronium, and hydrogen peroxide ice. In: Schenk, P., Nimmo, F., Prockter,

L.M. (Eds.), Workshop on Europa's Icy Shell: Past. Present, and Future, In: LPI Contribution CB-1195. Lunar and Planetary Institute, Houston. Abstract No. 7057.

Cooper, J.F., Johnson, R.E., Mauk, B.H., Garrett, H.B., Gehrels, N., 2001. Energetic ion and electron irradiation of the icy Galilean satellites. Icarus 149, 133–159.

Dose, K., BiegerDose, A., Dillmann, R., Kerz, O., Klein, A., Rolf, A., Stridde, C., 1996. UV photobiochemistry of anhydrobiotic organisms at extremely low temperatures. Adv. Space Res. 18, 69–74.

Duggan, D.E., Elliker, P.R., Anderson, A.W., 1963. Inactivation of radiation-resistant spoilage bacterium *Micrococcus radiodurans*. II. Radiation inactivation rates as influenced by menstruum temperature, preirradiation heat treatment, and certain reducing agents. Appl. Microbiol. 11 (5), 413–417.

Fagents, S.A., 2003. Considerations for effusive cryovolcanism on Europa: The post-Galileo perspective. J. Geophys. Res.-Planets 108 (E12), 5139.

Fagents, S.A., Greeley, R., Sullivan, R.J., Pappalardo, R.T., Prockter, L.M., 2000. Cryomagmatic mechanisms for the formation of Rhadamanthys linea, triple band margins, and other low-albedo features on Europa. Icarus 144 (1), 54–88.

Grundy, W.M., Schmitt, B., 1998. The temperature-dependent near-infrared absorption spectrum of hexagonal ice. J. Geophys. Res. 103, 25809–25822.

Hall, D.T., Feldman, P.D., McGrath, M.A., Strobel, D.F., 1998. The far-ultraviolet oxygen airglow of Europa and Ganymede. Astrophys. J. 499 (1), 475–481.

Hall, D.T., Strobel, D.F., Feldman, P.D., McGrath, M.A., Weaver, H.A., 1995. Detection of an oxygen atmosphere on Jupiter's moon Europa. Nature 373 (6516), 677–679.

Hapke, B., 1981. Bidirectional reflectance spectroscopy. I. Theory. J. Geophys. Res. 86, 3039–3054.

Hapke, B., 1993. Theory of reflectance and emittance spectroscopy. In: Arvidson, R.E., Rycroft, M.J. (Eds.), Topics in Remote Sensing, vol. 3. Cambridge Univ. Press, Cambridge, p. 455.

Head, J.W., Pappalardo, R.T., 1999. Brine mobilization during lithospheric heating on Europa: Implications for formation of chaos terrain, lenticula texture, and color variations. J. Geophys. Res.-Planets 104 (E11), 27143–27155.

Head, J.W., Pappalardo, R.T., Sullivan, R., 1999. Europa: Morphological characteristics of ridges and triple bands from Galileo data (E4 and E6) and assessment of a linear diapirism model. J. Geophys. Res.-Planets 104 (E10), 24223–24236.

Hendrix, A.R., Carlson, R.W., Mehlman, R., Smythe, W.D., 2002. Europa as measured by Galileo NIMS and UVS (abstract). In: Jupiter after Galileo and Cassini. Observatorio Astronomico de Lisboa, Lisbon, p. 108.

Hochanadel, C.J., Ghormley, J.A., Sworski, T.J., 1955. The decomposition of sulfuric acid by cobalt γ-rays. J. Am. Chem. Soc. 77, 3215.

Hosokawa, S., Matsuoka, T., Tamura, K., 1994. Optical absorption spectra of liquid sulphur over a wide absorption range. J. Phys. Condens. Matter 6, 5273–5282.

Imre, D.G., Xu, J., Tridico, A.C., 1997. Phase transformations in sulfuric acid aerosols: Implications for stratospheric ozone depletion. Geophys. Res. Lett. 24 (1), 69–72.

Johnson, R.E., 2000. Surface chemistry in the jovian magnetosphere radiation environment. In: Dressler, R.A. (Ed.), Chemical Dynamics in Extreme Environments, vol. 11. World Scientific, Singapore, pp. 390–419.

Johnson, R.E., Carlson, R.W., Cooper, J.F., Paranicas, C., Moore, M.H., Wong, M., 2004. Radiation effects on the surfaces of the Galilean satellites. In: Bagenal, F., McKinnon, W. (Eds.), Jupiter. Cambridge Univ. Press, Cambridge, pp. 485–512.

Johnson, R.E., Nelson, M.L., McCord, T.B., Gradie, J.C., 1988. Analysis of Voyager images of Europa—Plasma bombardment. Icarus 75 (3), 423–436.

Kargel, J.S., Head III, J.W., Hogenboom, D.L., Khurana, K.K., Marion, G., 2001. The system sulfuric acid-magnesium sulfate-water: Europa's ocean properties related to thermal state. Lunar Planet. Sci. XXXII. Abstract 2138 [CD-ROM].

Kargel, J.S., Kaye, J., Head, J.W.I., Marion, G., Sassen, R., Crowley, J., Prieto, O., Hogenboom, D., 2000. Europa's crust and ocean: Origin, composition, and prospects for life. Icarus 94, 368–390.

Lane, A.L., Nelson, R.M., Matson, D.L., 1981. Evidence for sulfur implantation in Europa's UV absorption band. Nature 292, 38–39.

Marion, G., 2002. A molal-based model for strong acid chemistry at low temperatures (187 to 298 K). Geochim. Cosmochim. Acta 66, 2499–2516.

McCord, T.B., Hansen, G.B., Fanale, F.P., Carlson, R.W., Matson, D.L., Johnson, T.V., Smythe, W.D., Crowley, J.K., Martin, P.D., Ocampo, A., Hibbitts, C.A., Granahan, J.C., 1998. Salts on Europa's surface detected by Galileo's Near Infrared Mapping Spectrometer. Science 280 (5367), 1242–1245.

McCord, T.B., Hansen, G.B., Matson, D.L., Johnson, T.V., Crowley, J.K., Fanale, F.P., Carlson, R.W., Smythe, W.D., Martin, P.D., Hibbitts, C.A., Granahan, J.C., Ocampo, A., NIMS Team, 1999. Hydrated salt minerals on Europa's surface from the Galileo NIMS investigation. J. Geophys. Res.-Planets 104, 11827–11851.

McCord, T.B., Teeter, G., Hansen, G.B., Sieger, M.T., Orlando, T.M., 2002. Brines exposed to Europa surface conditions. J. Geophys. Res. 107, 4-1–4-6.

McEwen, A.S., 1986. Exogenic and endogenic albedo and color patterns on Europa. J. Geophys. Res. 91, 8077–8097.

Moore, M.H., Hudson, R.L., Carlson, R.W., 2002. IR spectra of ion-irradiated ices containing SO_2 and H_2S. Bull. Am. Astron. Soc. 34. Abstract 902.

Mootz, D., Merschenz-Quack, A., 1987. On the highest hydrates of sulfuric acid: Formation and structure of $H_2SO_4 \cdot 6.5H_2O$ and $H_2SO_4 \cdot 8H_2O$. Z. Naturforsch. 42b, 1231–1236.

Nash, D.B., Fanale, F.P., 1977. Io's surface composition based on reflectance spectra of sulfur/salt mixtures and proton irradiation experiments. Icarus 31, 40–80.

Nimmo, F., Gaidos, E., 2002. Strike-slip motion and double ridge formation on Europa. J. Geophys. Res.-Planets 107 (E4), 5021.

Noll, K.S., Weaver, H.A., Gonnella, A.M., 1995. The albedo spectrum of Europa from 2200 angstrom to 3300 angstrom. J. Geophys. Res.-Planets 100 (E9), 19057–19059.

Ohtaki, H., Radnai, T., 1993. Structure and dynamics of hydrated ions. Chem. Rev. 93, 1157–1204.

Paranicas, C., Carlson, R.W., Johnson, R.E., 2001. Electron bombardment of Europa. Geophys. Res. Lett. 28 (4), 673–676.

Richmond, R.C., Sridhar, R., Zhou, Y., Daly, M.J., 1999. Physico-chemical survival pattern for the radiophile *D. radiodurans*: A polyextremophile model for life on Mars. In: Hoover, R.B. (Ed.), Instruments, Methods, and Missions for Astrobiology II. In: Proc. SPIE, vol. 3755. SPIE Press, Bellingham, WA, pp. 210–222.

Schmitt, B., Quirico, E., Trotta, F., Grundy, W.M., 1998. Optical properties of ices from UV to infrared. In: Schmitt, B., de Bergh, C., Festou, M. (Eds.), Solar System Ices. In: Astrophys. Space Sci. Library, vol. 227. Kluwer Academic, Norwell, MA, pp. 199–240.

Schriver-Mazzuoli, L., Schriver, A., Chaabouni, H., 2003. Photo-oxidation of SO_2 and of SO_2 trapped in amorphous water ice studied by IR spectroscopy. Implications for Jupiter's satellite Europa. Can. J. Phys. 81 (1–2), 301–309.

Silverman, G.J., 1991. Sterilization and preservation by ionizing radiation. In: Block, S.S. (Ed.), Disinfection Sterilization and Preservation. Lea and Febiger, Philadelphia, pp. 556–579.

Spencer, J.R., Calvin, W.M., 2002. Condensed O-2 on Europa and Callisto. Astron. J. 124 (6), 3400–3403.

Spencer, J.R., Grundy, W.M., Dumas, C., Carlson, R.W., McCord, T.B., Terrille, R., 2005. The nature of Europa's non-ice surface components: High spatial and spectral resolution spectroscopy from the Keck telescope. Icarus. In preparation.

Spencer, J.R., Klesman, A., 2001. New observations of molecular oxygen on Europa and Ganymede. Bull. Am. Astron. Soc. 33. Abstract 1125.

Spencer, J.R., Tampari, L.K., Martin, T.Z., Travis, L.D., 1999. Temperatures on Europa from Galileo photopolarimeter–radiometer: Nighttime thermal anomalies. Science 284, 1514–1516.

Tiscareno, M.S., Geissler, P.E., 2003. Can redistribution of material by sputtering explain the hemispheric dichotomy of Europa? Icarus 161, 90–101.

Tisdale, R.T., Glandorf, D.L., Tolbert, M.A., Toon, O.B., 1998. Infrared optical constants of low-temperature H_2SO_4 solutions representative of stratospheric sulfate aerosols. J. Geophys. Res.-Atmospheres 103 (D19), 25353–25370.

Van De Hulst, H.C., 1980a. Multiple Light Scattering and Radiative Transfer, vol. 1. Academic Press, New York.

Van De Hulst, H.C., 1980b. Multiple Light Scattering and Radiative Transfer, vol. 2. Academic Press, New York.

Zahnle, K., Dones, L., Levison, H.F., 1998. Cratering rates on the Galilean satellites. Icarus 136, 202–222.

Zahnle, K., Schenk, P., Levison, H., Dones, L., 2003. Cratering rates in the outer Solar System. Icarus 163 (2), 263–289.

Zeleznik, F.J., 1991. Thermodynamic properties of the aqueous sulfuric acid system to 350-K. J. Phys. Chem. Ref. Data 20 (6), 1157–1200.

Zeleznik, F.J., 1994. Thermodynamic properties of the aqueous sulfuric acid system to 350-K (vol. 20, Pg. 1157, 1991). J. Phys. Chem. Ref. Data 23 (1), 155–155 (Errata).